Composite Structures 208 (2019) 78–90

Contents lists available at ScienceDirect

Composite Structures

journal homepage: www.elsevier.com/locate/compstruct

Vibration characteristics of a rotating pre-twisted composite laminated blade

Jie Chen[a,b], Qiu-Sheng Li[a,b,*]

[a] Department of Architecture and Civil Engineering, City University of Hong Kong, Kowloon, Hong Kong, China
[b] Architecture and Civil Engineering Research Center, City University of Hong Kong Shenzhen Research Institute, Shenzhen, PR China

ARTICLE INFO

Keywords:
Rotating pre-twisted blade
Composite laminated structure
Vibration characteristics
Free vibration
Frequency loci veering

ABSTRACT

A new dynamic model based on the shell theory is presented to investigate the vibration behavior of a rotating composite laminated blade with a pre-twisted angle. The effects of the Coriolis and centrifugal forces due to the rotation motion of the blade are considered in the formulation. Based on the Rayleigh-Ritz method and continuous algebraic polynomial functions satisfying the boundary conditions of a cantilever, the natural frequencies and mode shapes of a rotating pre-twisted blade are obtained. The convergence analysis is performed and the accuracy of the proposed model is verified by comparing the non-dimensional frequencies obtained by the present method with those in literature. The frequency loci veering and crossing phenomena along with the corresponding mode shape variations are presented and discussed in detail. A comprehensive parameter investigation of the effects of aspect ratio, pre-twisted angle, stagger angle, rotation velocity and hub radius on variations of the modal characteristics of the blade is conducted. It is demonstrated through the results of this paper that the developed model is effective to evaluate the dynamic behavior of rotating pre-twisted blades, which would be useful for improvement in design and optimization of the material and geometry dimension of the blades.

1. Introduction

Rotating structures are widely used as key components in various engineering applications, such as blades of turbines, helicopters and aircraft engines. The vibration or modal characteristics of blades change significantly when the structures undergo overall motions. For example, centrifugal inertia forces lead to the stretching of the structures and increase their bending stiffness, while Coriolis effects produce vibration couplings between different vibration modes and generate complex vibration mode shapes [1]. Analytical or semi-analytical methods are desirable to understand and identify the dynamic properties of blades with good accuracy at low computational costs.

Beam models have extensively been adopted to analyze the dynamic response of a rotating blade in many literatures. Such idealization could provide accurate dynamic characteristics for most rotating structures. For example, Yao et al. [2,3] treated a rotating blade as a pre-twisted, presetting and thin-walled rotating cantilever beam under varying rotating speed. The nonlinear dynamic responses of the rotating blade under high-temperature supersonic gas flow was investigated. Lee et al. [4,5] studied the free vibration of a beam rotating at a constant angular velocity. They revealed the effects of the setting angle on the natural frequencies of pre-twisted beams. Liu and Ren [6] analyzed the dynamic characteristics of a wind turbine rotor blade by regarding it as a composite anisotropic thin-walled closed-section beam. Yoo et al. [7] used the Rayleigh-Ritz method to study the vibration characteristics of a rotating pre-twisted blade with a concentrated mass. Librescu et al. [8–10] investigated the modeling and free vibration of pre-twisted rotating blades made of functionally graded materials (FGMs) and operating in a high-temperature field. The blade is modeled as a thin-walled beam that incorporates the pre-twisted effects. Lin and Chen [11] investigated the stability problem of spinning pre-twisted sandwich beams subjected to periodic axial load. Other previous studies [12,13] primarily dealt with the free vibration characteristics of twisted rotating beams, which also included the effect of transverse shear and rotary inertia. Hajianmaleki and Qatu [14,15] presented a review of composite beam modeling approach for analyzing anisotropic blades.

However, the beam models are not suitable for blades with low aspect ratios and high frequencies which are widely encountered in real engineering practices. Besides, the beam models are unable to predict the blade vibrational mode associated with the chordwise bending and the coupled spanwise and chordwise bending [16]. Hence, attempts have been made to formulate the dynamic behavior of rotating blades

* Corresponding author at: Department of Architecture and Civil Engineering, City University of Hong Kong, Kowloon, Hong Kong, China.
E-mail address: bcqsli@cityu.edu.hk (Q.-S. Li).

https://doi.org/10.1016/j.compstruct.2018.10.005
Received 28 May 2018; Received in revised form 18 September 2018; Accepted 4 October 2018
Available online 06 October 2018
0263-8223/

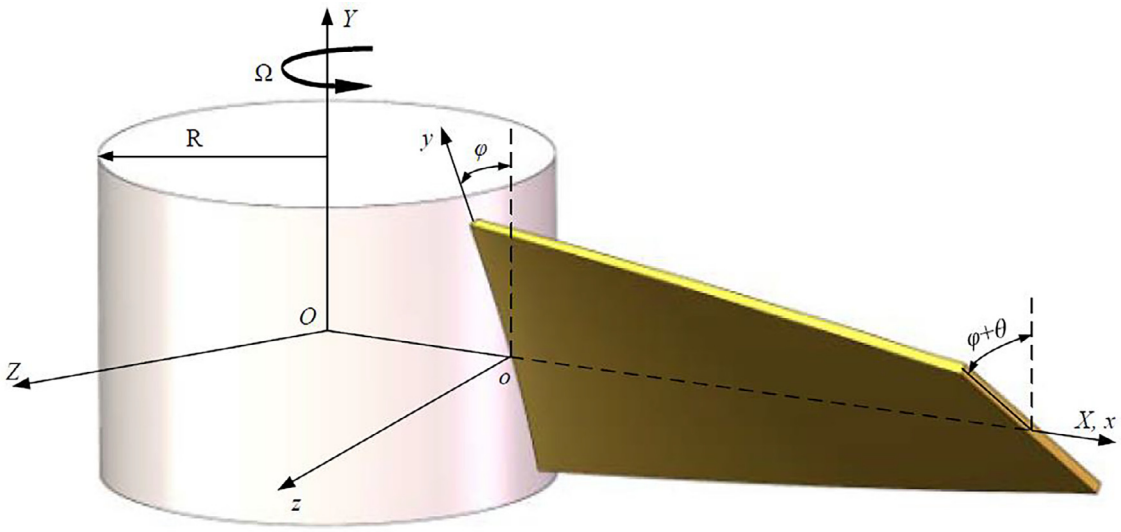

Fig. 1. Configuration of a composite laminated pre-twisted blade model.

with the plate theory. By applying the Rayleigh-Ritz method, Yoo et al. [17,18] derived a set of linear equations of motion for the modal analysis of rotating cantilevered plates. The frequency loci veering and crossing phenomena along with the corresponding mode shape variations were observed and discussed. Fang et al. [19] investigated the free vibration of rotating rectangular Mindlin plates with variable thickness by using the Chebyshev–Ritz method. Mindlin plates theory has also been applied for the analysis of rotating thick plates in [20,21], which can improve the accuracy of the modal analysis by considering the effects of shear deformation and rotary inertia. Hashemi et al. [22] developed a finite element formulation for the vibration analysis of rotating thick plates by considering Coriolis effects and couplings between in-plane and out-plane deformations. Modal analysis of a rotating thin plate was conducted by Zhao et al. [23] through the use of the thin plate elements described by the absolute nodal coordinate formulation. Sun et al. [24] developed a dynamic model based on the plate theory to investigate the vibration behavior of a rotating blade. Two types of excitation forces were considered to study the peak reductions at resonances with damping effect. Li and Zhang [25] developed a dynamic model of a functionally graded rectangular plate undergoing large overall motions. The effects of dimensionless parameters such as hub radius ratio, aspect ratio, and volume fraction exponent on the variations of the natural frequencies were investigated

When the influences of curvature and pre-twisted angle are considered, the shell models are more appropriate and accurate for rotating blades. Jang and Kim [26] experimentally showed the curvature effect on the dynamic response of composite airfoils. Sun et al. [27,28] established a dynamic model for a pre-twisted rotating blade mounted at an arbitrary stagger angle by applying the general shell theory. The rotational velocity was considered in their model to study the eigenfrequencies and damping properties of the pre-twisted rotating blade. Sinha [29] modeled a twisted airfoil as a thin shell with suitable camber radius of the curved surface. The numerical results were directly applicable to determine the static and running frequencies of typical composite blades used in the fan module of an aeroengine. Kee and Kim [30] derived a general formulation for an initially twisted rotating shell structures including the effect of centrifugal force and Coriolis acceleration. The effects of the curving and twisting on the vibrations of a rotating blade during complex rotation were studied by Gulyaev and Khudolii [31]. It was found that these geometrical factors may cause additional resonant vibrations. Zhang [32] used a wave propagation approach to study the frequency of rotating composite cylindrical shells. The effects of different shell parameters and boundary conditions on the frequencies were investigated.

To the author's knowledge, there is a lack of research works devoted to vibration analysis of a rotating blade made up of composite laminated materials based on the shell theory. In this paper, a novel structural model is developed to study the free vibration characteristics of a pre-twisted composite laminated blade mounted at an arbitrary stagger angle. The shell theory is applied to derive the equations for the modal analysis by considering the effects of centrifugal and Coriolis. The accuracy of the proposed model is verified against the results in literature and from ANSYS. A comprehensive parameter investigation of the effects of the aspect ratio, pre-twisted angle, stagger angle, hub radius on the variations of the modal characteristics is performed. Frequency loci veering and crossing phenomena are observed and discussed in detail.

It is demonstrated through the results of this paper that the developed model is effective to evaluate the dynamic behavior of rotating pre-twisted blades, which would be useful for the design and optimization of the blades.

2. Mathematical formulation

2.1. Basic equations

A composite laminated blade with a uniform mass distribution is modeled as a pre-twisted curved panel which is clamped to a rigid disk with a radius R and mounted with setting angle φ, as shown in Fig. 1. The geometric parameters of the blade are represented by the span length L, the chord length b, the thickness h and the angular rotating velocity about the rigid disk axis Ω.

In this paper, two coordinate systems are established. One is the Cartesian coordinate system XYZ with the unit vectors ($\mathbf{i}_X$, $\mathbf{i}_Y$, $\mathbf{i}_Z$), which is attached to the central line of the disk. The other is the xyz coordinate system with the unit vectors ($\mathbf{i}_x$, $\mathbf{i}_y$, $\mathbf{i}_z$), where the origin lies at the root of the mid-surface of the blade. The x-axis is parallel to the X-axis, the y-axes can be obtained by rotating around the x-axis with the setting angle φ starting from the Y-axis direction. θ is the twist angle at the free end of the blade.

$$\theta(x) = qx \tag{1}$$

where q is the uniform varying rate of the twist angle.

To describe the twisted surface of the blade, an orthogonal coordinate system $ox\eta\zeta$ can be defined [33,34]. The η-axis is tangent to the blade surface, rotating at a constant twist rate $\theta' = \theta/L$, and is always orthogonal to the x-axis. The ζ-axis is the normal vector to blade surface, which is the cross product of the x and ζ axis. Hence, the position

Table 1
Comparison of the first five non-dimensional frequencies.

Mode	Present method	Ref [30]
1	5.25	5.26
2	8.62	8.61
3	25.08	25.07
4	28.44	28.46
5	43.87	43.84

vector $\mathbf{r}_0(x, \eta)$ of an arbitrary point in the mid-surface of the pre-twisted blade in $x\eta$-coordinate can be determined by

$$\mathbf{r}_0 = \begin{bmatrix} x \\ \eta\cos\theta \\ \eta\sin\theta \end{bmatrix}^T \begin{pmatrix} \mathbf{i}_x \\ \mathbf{i}_y \\ \mathbf{i}_z \end{pmatrix} \tag{2}$$

The corresponding unit vectors ($\mathbf{e}_{0x}$, $\mathbf{e}_{0\eta}$, $\mathbf{e}_{0\zeta}$) along each orthogonal coordinate can be expressed as

$$\mathbf{e}_{0j} = \begin{pmatrix} \mathbf{e}_{0x} \\ \mathbf{e}_{0\eta} \\ \mathbf{e}_{0\zeta} \end{pmatrix} = \begin{pmatrix} \frac{r_{0,x}}{|r_{0,x}|} \\ \frac{r_{0,\eta}}{|r_{0,\eta}|} \\ \mathbf{e}_{0x}\cdot\mathbf{e}_{0\eta} \end{pmatrix} = \frac{1}{A}\begin{bmatrix} 1 & -\eta q\sin\theta & \eta q\cos\theta \\ 0 & A\cos\theta & A\sin\theta \\ -\eta q & -\sin\theta & \cos\theta \end{bmatrix} \begin{pmatrix} \mathbf{i}_x \\ \mathbf{i}_y \\ \mathbf{i}_z \end{pmatrix} \tag{3}$$

where A is the Lame parameters of the middle surface in the x direction [35], given by

$$A = |r_{0,x}| = \sqrt{1 + q^2\eta^2} \tag{4}$$

Eq. (2) can be used to describe the deformation field on the blade under the condition of small blade thickness [33]. However, this simplification will influence the accuracy to some extent, especially at large twist angles or large thickness [27]. An arbitrary material point in the volume of the pre-twisted blade can be expressed by a position vector $\mathbf{r}_1$ with including the normal axis ζ

$$\mathbf{r}_1 = \mathbf{r}_0 + \zeta\mathbf{e}_{0\zeta} = \frac{1}{A}\begin{bmatrix} Ax - \eta\zeta q \\ A\eta\cos\theta - \zeta\sin\theta \\ A\eta\sin\theta + \zeta\cos\theta \end{bmatrix}^T \begin{pmatrix} \mathbf{i}_x \\ \mathbf{i}_y \\ \mathbf{i}_z \end{pmatrix} \tag{5}$$

The displacement vector $\mathbf{r}_2$ can be written as

$$\mathbf{r}_2 = [u \quad v \quad w]\begin{pmatrix} \mathbf{e}_{0x} \\ \mathbf{e}_{0\eta} \\ \mathbf{e}_{0\zeta} \end{pmatrix} = \frac{1}{A}\begin{bmatrix} u - \eta w q \\ Av\cos\theta - (q\eta u + w)\sin\theta \\ Av\sin\theta + (q\eta u + w)\cos\theta \end{bmatrix}^T \begin{pmatrix} \mathbf{i}_x \\ \mathbf{i}_y \\ \mathbf{i}_z \end{pmatrix} \tag{6}$$

An arbitrary point of the blade after deformation can be expressed by the position vector $\mathbf{r}$

$$\mathbf{r} = \mathbf{r}_1 + \mathbf{r}_2 = \frac{1}{A}\begin{bmatrix} Ax + u - \eta q(\zeta + w) \\ A(\eta + v)\cos\theta - (u\eta q + \zeta + w)\sin\theta \\ A(\eta + v)\sin\theta + (u\eta q + \zeta + w)\cos\theta \end{bmatrix}^T \begin{pmatrix} \mathbf{i}_x \\ \mathbf{i}_y \\ \mathbf{i}_z \end{pmatrix} \tag{7}$$

2.2. Strain energy

The displacement field of the pre-twisted blade can be expressed as

$$u_0(x, \eta, \zeta, t) = u(x, \eta, t) - \zeta\frac{\partial w(x, \eta, t)}{\partial x} \tag{8}$$

$$v_0(x, \eta, \zeta, t) = v(x, \eta, t) - \zeta\frac{\partial w(x, \eta, t)}{\partial \eta} \tag{9}$$

$$w_0(x, \eta, \zeta, t) = w(x, \eta, t) \tag{10}$$

where u, v and w are the displacements of points on the middle surface of the curved panel in x, η and ζ direction.

The strain components ε_{xx}, $\varepsilon_{\eta\eta}$ and $\gamma_{x\eta}$ at an arbitrary point of the curved panel are corresponding to the middle surface strains ε_{x0}, $\varepsilon_{\eta 0}$ and $\gamma_{x\eta 0}$, and to the changes in the curvature and torsion of the middle surface k_x, k_η and $k_{x\eta}$ by the following relations

$$\varepsilon_x = \varepsilon_{x0} + \zeta k_x \tag{11}$$

$$\varepsilon_\eta = \varepsilon_{\eta 0} + \zeta k_\eta \tag{12}$$

$$\gamma_{x\eta} = \gamma_{x\eta 0} + \zeta k_{x\eta} \tag{13}$$

where the strain-displacement relationships at the middle surface on a curved panel are expressed as [36]

$$\varepsilon_{x0} = \frac{\partial u}{\partial x} + \frac{w}{R_x} + \frac{1}{2}\left(\frac{\partial w}{\partial \eta}\right)^2 \tag{14}$$

$$\varepsilon_{\eta 0} = \frac{\partial v}{\partial \eta} + \frac{w}{R_\eta} + \frac{1}{2}\left(\frac{\partial w}{\partial \eta}\right)^2 \tag{15}$$

$$\gamma_{x\eta 0} = \frac{\partial u}{\partial \eta} + \frac{\partial v}{\partial x} + \frac{2w}{R_{x\eta}} + \frac{\partial w}{\partial x}\frac{\partial w}{\partial \eta} \tag{16}$$

where R_x and R_η are the radii of curvature in x and η direction, respectively, and $R_{x\eta}$ is the radius of torsion. These coefficients can be derived based on the differential geometry theory [37]

$$\frac{1}{R_x} = 0, \quad \frac{1}{R_\eta} = 0, \quad \frac{1}{R_{x\eta}} = -\frac{q}{A^2} \tag{17}$$

The changes in the curvature and torsion of the reference surface are given as

$$k_x = -\frac{\partial^2 w}{\partial x^2} \tag{18}$$

$$k_\eta = -\frac{\partial^2 w}{\partial \eta^2} \tag{19}$$

$$k_{x\eta} = -2\frac{\partial^2 w}{\partial x \partial \eta} \tag{20}$$

The stress-strain relationship of the symmetric cross-ply laminated composite panel can be obtained [38]

$$\begin{Bmatrix} \sigma_x \\ \sigma_\eta \\ \sigma_{x\eta} \end{Bmatrix}^{(k)} = \begin{bmatrix} Q_{11} & Q_{12} & 0 \\ Q_{21} & Q_{22} & 0 \\ 0 & 0 & Q_{66} \end{bmatrix}^{(k)} \begin{Bmatrix} \varepsilon_x \\ \varepsilon_\eta \\ \varepsilon_{x\eta} \end{Bmatrix}^{(k)} \tag{21}$$

where k donates the layer number.

The coefficients of material tensor Q_{ij} are given by

Table 2
Comparison of the first five non-dimensional frequencies.

Mode	3× 5 × 5	3× 6 × 6	3× 7 × 7
1	3.3507	3.3638	3.3627
2	19.735	19.933	19.896
3	50.027	50.132	50.164
4	50.516	51.021	51.115
5	58.162	58.256	58.249
6	75.533	75.6843	75.6531

Table 3
Comparison of the first five non-dimensional frequencies.

Mode	Present method	ANSYS
1	9.8810	9.8811
2	25.103	25.105
3	60.589	60.583
4	69.597	69.592
5	90.339	90.334

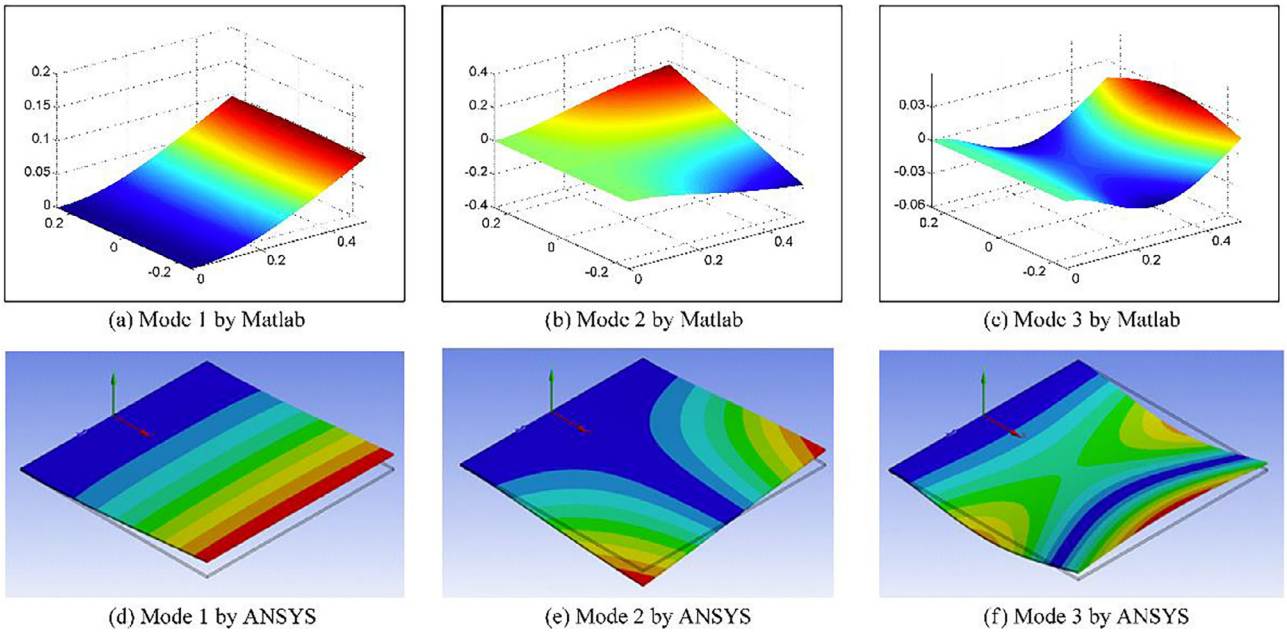

Fig. 2. Mode shapes of the pre-twisted blade, (a) first order and (b) second order and (c) third order mode shape by the present method (Matlab); (d) first order and (e) second order and (f) third order mode shape by ANSYS.

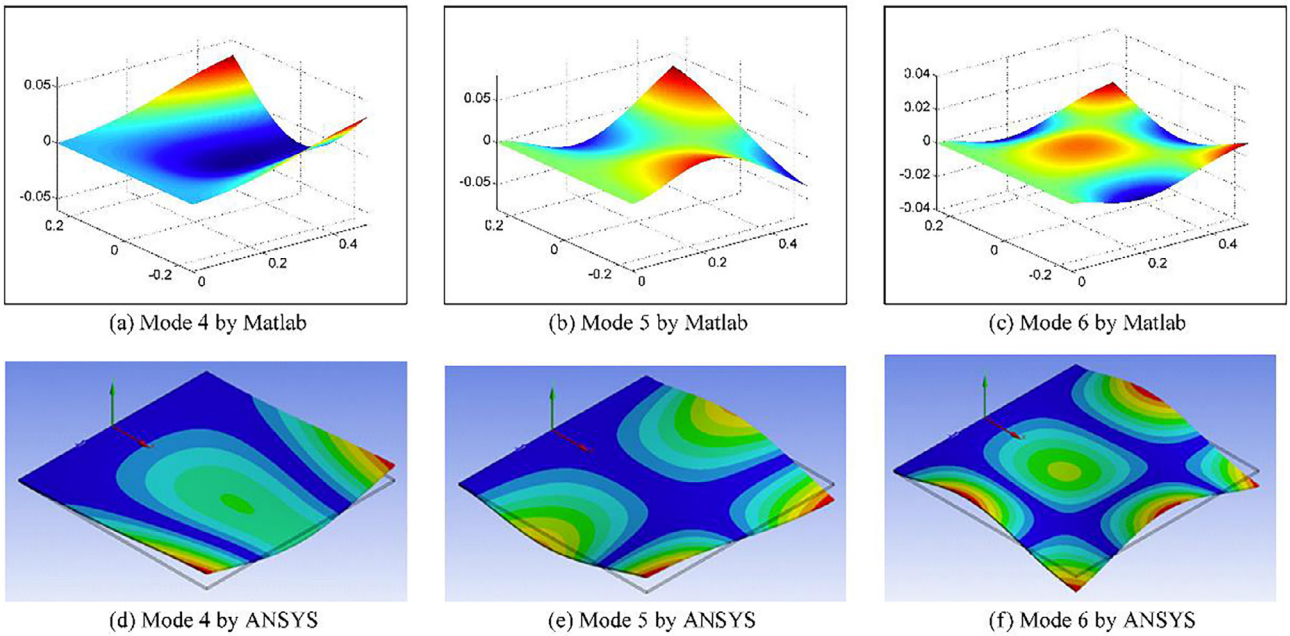

Fig. 3. Mode shapes of the pre-twisted blade, (a) fourth order and (b) fifth order and (c) sixth order mode shape by the present method (Matlab); (d) fourth order and (e) fifth order and (f) sixth order mode shape by ANSYS.

$$Q_{11} = \frac{E_1}{1-\upsilon_{12}\upsilon_{21}},\ Q_{12} = Q_{21} = \frac{\upsilon_{12}E_1}{1-\upsilon_{12}\upsilon_{21}},\ Q_{22} = \frac{E_2}{1-\upsilon_{12}\upsilon_{21}},\ Q_{66} = G_{12} \tag{22}$$

where E_1 and E_2 represent the Young's Modulus in the two in-plane directions, υ_{12} and υ_{21} are the associated with the two in-plane Poisson ratios, and G_{12} is the in-plane shear modulus.

The extensional stiffness A_{ij}, bending stiffness D_{ij}, and bending-extensional coupling stiffnesses are defined in terms of Q_{ij} as

$$(A_{ij},\ B_{ij},\ D_{ij}) = \int_{-h/2}^{h/2} Q_{ij}(1,\ \zeta,\ \zeta^2)\quad d\zeta\,(i,\ j = 1,\ 2,\ 6) \tag{23}$$

By assuming null contributions of transverse shear and through-thickness normal deformation to the strain energy, the strain energy is defined as

$$U_S = \frac{1}{2}\iint_s \int_{-h/2}^{h/2} (\sigma_x\varepsilon_x + \sigma_\eta\varepsilon_\eta + \sigma_{x\eta}\gamma_{x\eta})\,dxd\eta d\zeta \tag{24}$$

Substituting Eqs. (21)–(23) into Eq. (24), yield the following expression

$$\begin{aligned} U_S = \frac{1}{2}\iint_s [&(A_{11}\varepsilon_{x0}^2 + 2B_{11}\varepsilon_{x0}k_x + D_{11}k_x^2) \\ &+ (A_{22}\varepsilon_{\eta0}^2 + 2B_{22}\varepsilon_{\eta0}k_\eta + D_{22}k_\eta^2) + (A_{66}\gamma_{x\eta0}^2 + B_{66}\gamma_{x\eta0}k_{x\eta} + D_{66}k_{x\eta}^2) \\ &+ 2(A_{12}\varepsilon_{x0}\varepsilon_{\eta0} + B_{12}\varepsilon_{x0}k_\eta + B_{12}\varepsilon_{\eta0}k_x + D_{12}k_xk_\eta)]\,dxd\eta d\zeta \end{aligned} \tag{25}$$

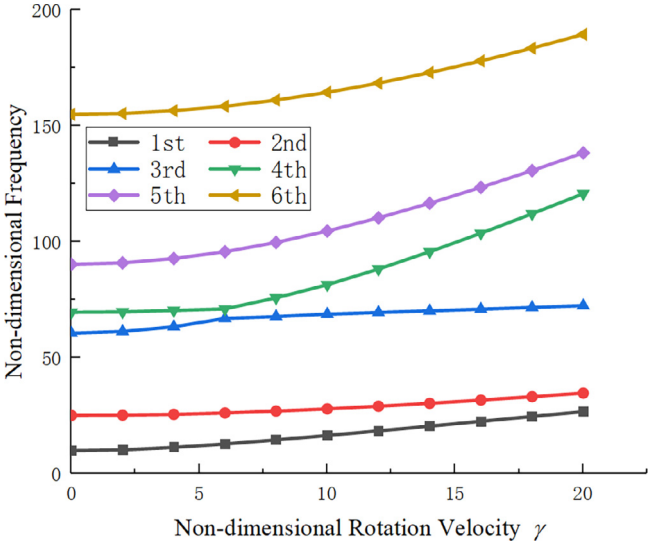

Fig. 4. First six non-dimensional frequencies of the blade versus rotation velocity. ($\delta = 1$, $\sigma = 0$, $\lambda = 0.01$, $\theta = 0°$ and $\varphi = 0°$).

2.3. Potential energy of centrifugal force

It is known that under high speed rotation the pre-twisted blade will be affected by centrifugal force and cause the centrifugal stiffening effect. This factor should be included when the vibration characteristics of the blade are analyzed. The coordinate system transformation relationship between the *xyz*-coordinate and *XYZ*-coordinate is given by

$$\begin{pmatrix}\mathbf{i}_x\\ \mathbf{i}_y\\ \mathbf{i}_z\end{pmatrix} = \begin{bmatrix}1 & 0 & 0\\ 0 & \cos\varphi & \sin\varphi\\ 0 & \sin\varphi & \cos\varphi\end{bmatrix}\begin{pmatrix}\mathbf{i}_X\\ \mathbf{i}_Y\\ \mathbf{i}_Z\end{pmatrix} \tag{26}$$

Then, the angular velocity $\mathbf{\Omega}$ in the *xyz*-coordinate of the curved panel is expressed as

$$\mathbf{\Omega} = \begin{bmatrix}0\\ \Omega\cos\varphi\\ -\Omega\sin\varphi\end{bmatrix}\begin{pmatrix}\mathbf{i}_x\\ \mathbf{i}_y\\ \mathbf{i}_z\end{pmatrix} \tag{27}$$

In the above equation, the width component of the angular velocity $\Omega\cos\varphi$ produces centrifugal forces in the longitudinal direction, and the thickness component $-\Omega\sin\varphi$ generates a torque about the longitudinal axis, which has a tendency to reduce the twist angle θ [16,29]. The corresponding centrifugal force components $\mathbf{F}_c$ of per unit volume in the blade is given by

$$\mathbf{F}_c = \rho\mathbf{\Omega}\times(\mathbf{r}_1 + R\mathbf{i}_x)\times\mathbf{\Omega} = \rho\Omega^2\begin{bmatrix}R + x - \frac{\zeta\eta k}{A}\\ \eta\sin\psi\sin\theta + \frac{\zeta}{A}\cos\psi\sin\theta\\ \eta\sin\psi\cos\theta + \frac{\zeta}{A}\cos\psi\cos\theta\end{bmatrix}^T\begin{pmatrix}\mathbf{i}_x\\ \mathbf{i}_y\\ \mathbf{i}_z\end{pmatrix} \tag{28}$$

in which $\psi = \varphi + \theta$ is the sum of setting angle and the twist angle, respectively.

The rotation of the blade about the axial direction results in membrane stresses, which are essentially acting in the radial direction (the width direction and the length direction of the blade). Projecting those force components into the ($\mathbf{e}_{0x}$ $\mathbf{e}_{0\eta}$ $\mathbf{e}_{0\zeta}$) coordinates, the new centrifugal force components in the orthogonal coordinate system are given [27]

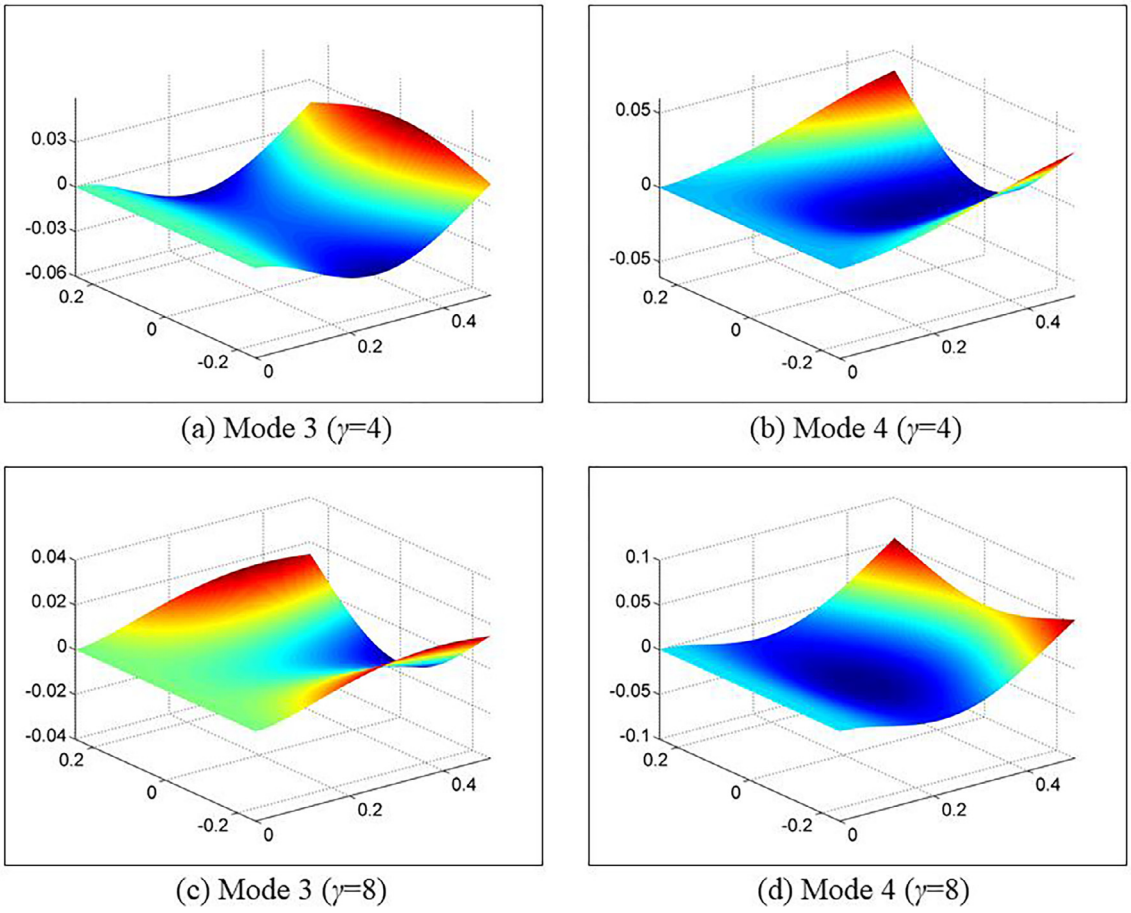

Fig. 5. Mode shapes of the pre-twisted blade, (a) third order and (b) fourth mode with $\gamma = 4$; (c) third mode and (d) fourth order mode shapes with $\gamma = 8$.

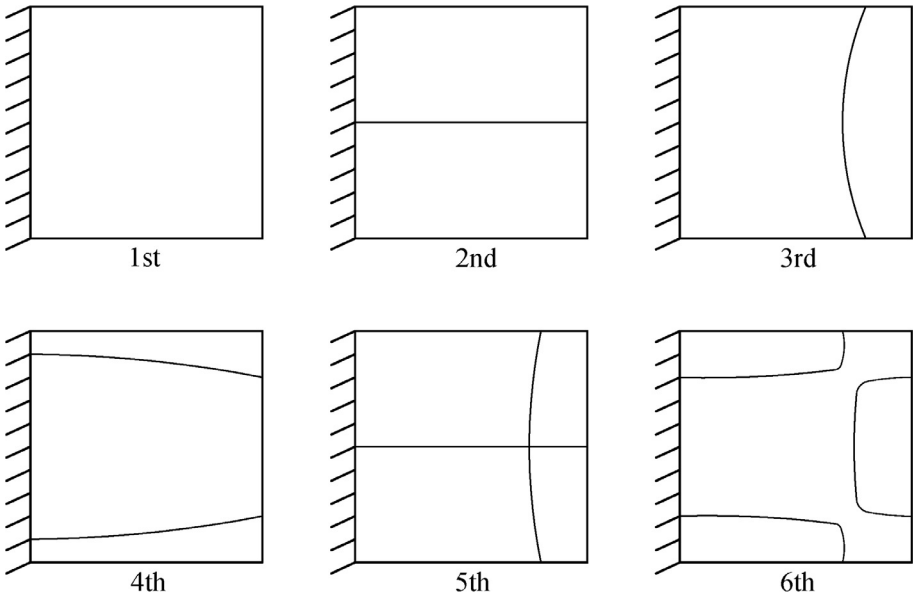

Fig. 6. First six nodal line patterns of the pre-twisted blade with $\gamma = 4$.

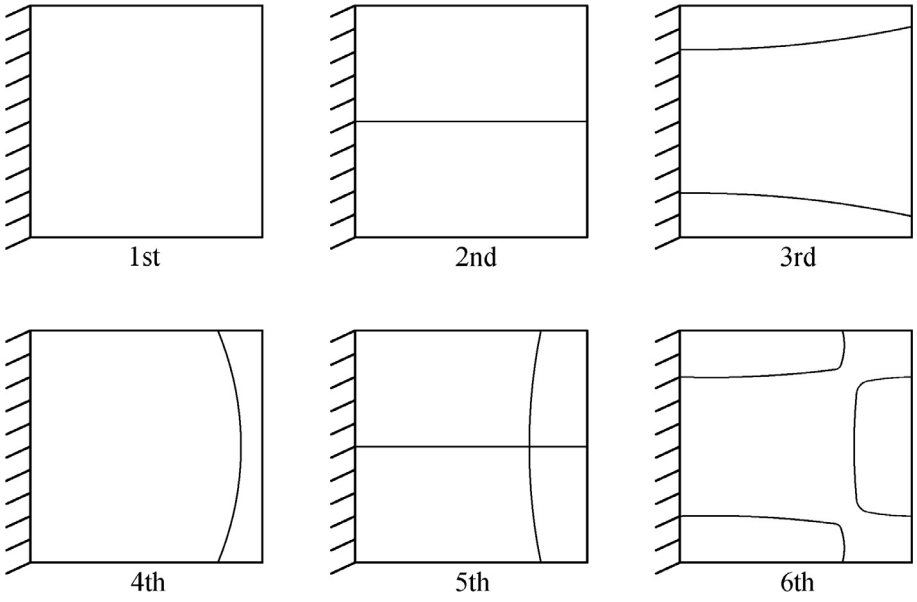

Fig. 7. First six nodal line patterns of the pre-twisted blade with $\gamma = 8$.

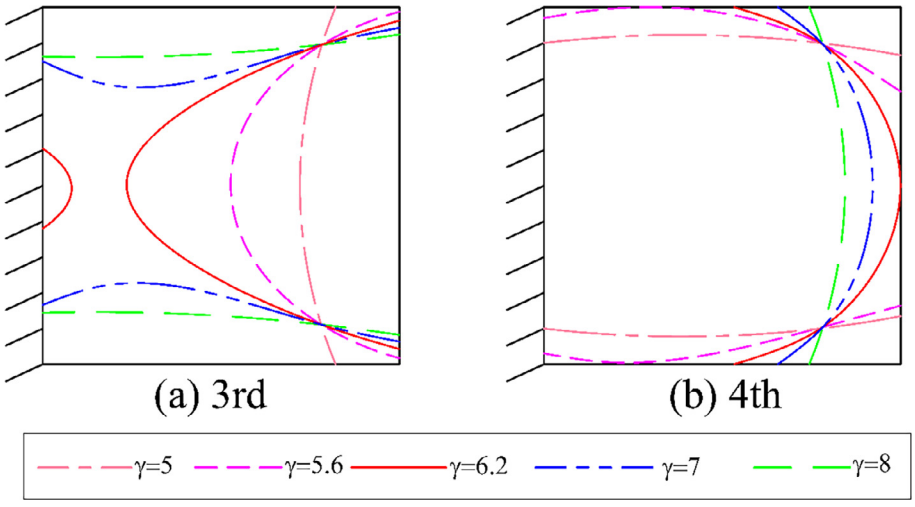

Fig. 8. Variation of the nodal lines of the third and fourth mode shapes versus non-dimensional rotation velocity.

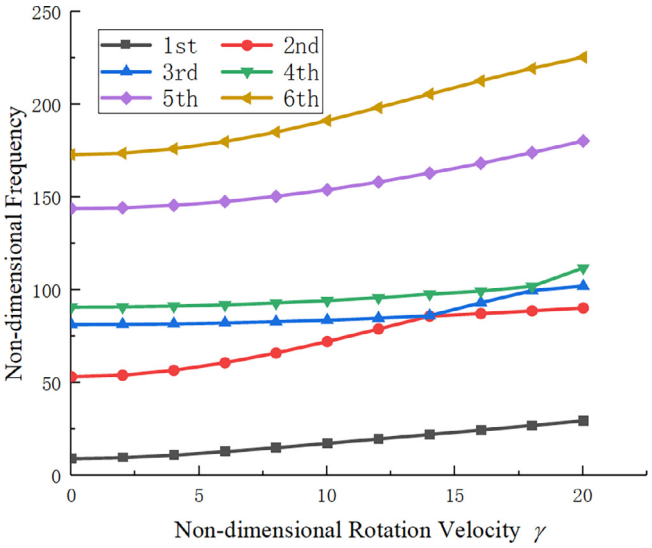

Fig. 9. First six non-dimensional frequencies of the pre-twisted blade versus non-dimensional rotation velocity with $\theta = 45°$.

$$\mathbf{N}_c = \begin{bmatrix} N_1 \\ N_2 \\ N_3 \end{bmatrix} = \begin{bmatrix} \int_0^L \mathbf{F}_c \cdot \mathbf{e}_{0x} A dx \\ \int_0^b \mathbf{F}_c \cdot \mathbf{e}_{0\eta} A d\eta \\ \int_{-h/2}^{h/2} \mathbf{F}_c \cdot \mathbf{e}_{0\zeta} A d\zeta \end{bmatrix} \tag{29}$$

Similar to derivation in Eq. (24), we assume null transverse shear and normal strains. Consequently, the centrifugal potential energy can be written as

$$U_{CF} = \frac{1}{2} \iint_s \int_{-h/2}^{h/2} (N_1 \varepsilon_{cs} + N_2 \varepsilon_{cc})\, dx d\eta d\zeta \tag{30}$$

where the longitudinal component N_1 of the centrifugal forces results in stiffening of the blade, and the width component N_2 leads to softness of the blade by untwisting the cross-section of the blade. ε_{cs} and ε_{cc} are the corresponding displacement components caused by the centrifugal force components N_1 and N_2, which are expressed as [24]

$$\varepsilon_{cs} = \frac{1}{2}\left(\frac{\partial w}{\partial x}\right)^2 + \frac{1}{2}\left(\frac{\partial v}{\partial x}\right)^2, \quad \varepsilon_{cc} = \frac{1}{2}\left(\frac{\partial w}{\partial \eta}\right)^2 + \frac{1}{2}\left(\frac{\partial u}{\partial \eta}\right)^2 \tag{31}$$

The total potential energy can be written as

$$U = U_S + U_{CF} \tag{32}$$

2.4. Kinetic energy

The velocity $\mathbf{V}_r$ of a point due to the rotation can be derived as [27]

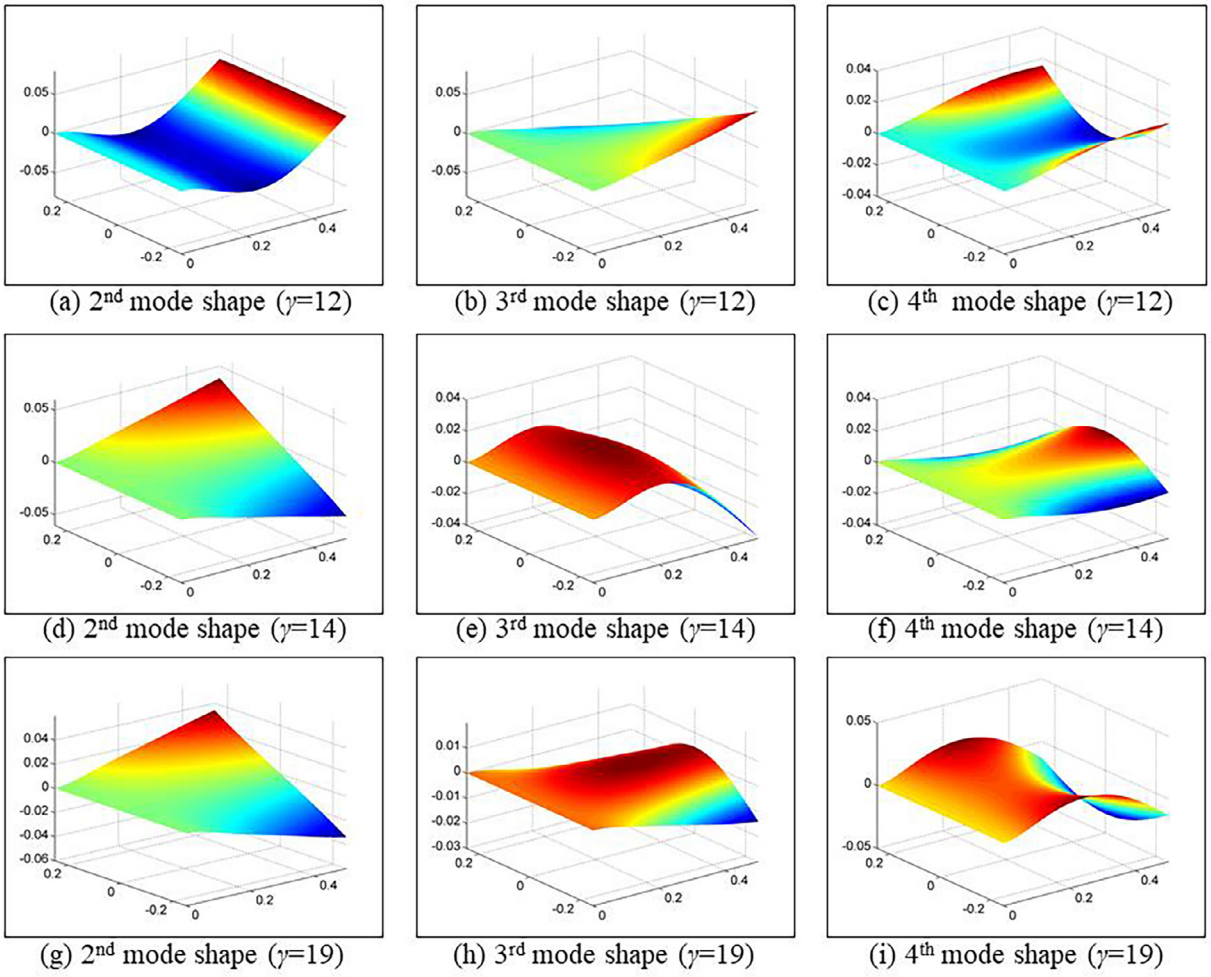

Fig. 10. Mode shapes of the pre-twisted blade, (a) second order and (b) third mode and (c) fourth order mode shapes with $\gamma = 12$; (d) second order and (e) third mode and (f) fourth order mode shapes with $\gamma = 14$; (g) second order and (h) third mode and (i) fourth order mode shapes with $\gamma = 19$.

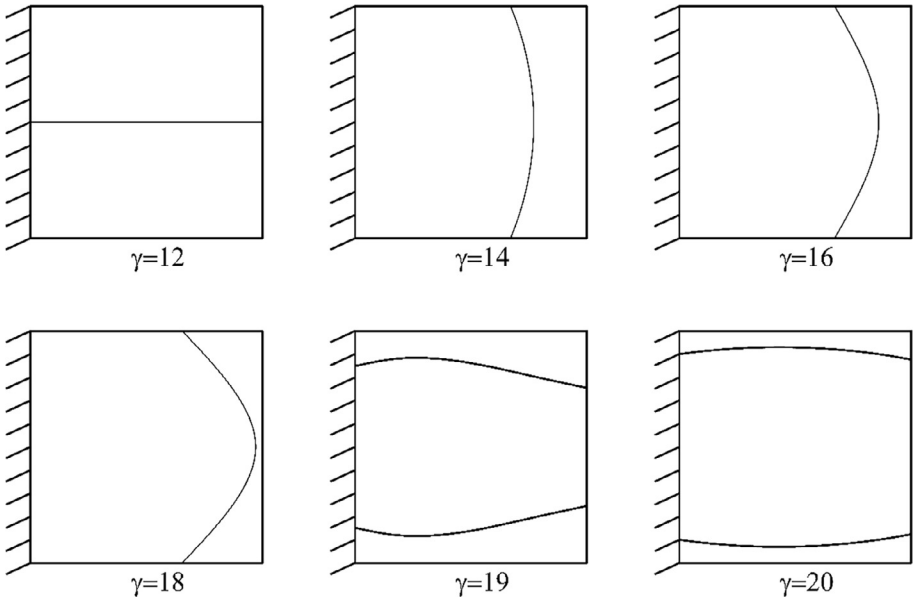

Fig. 11. Variation of the nodal line of the third mode shape with an increase of rotation velocity.

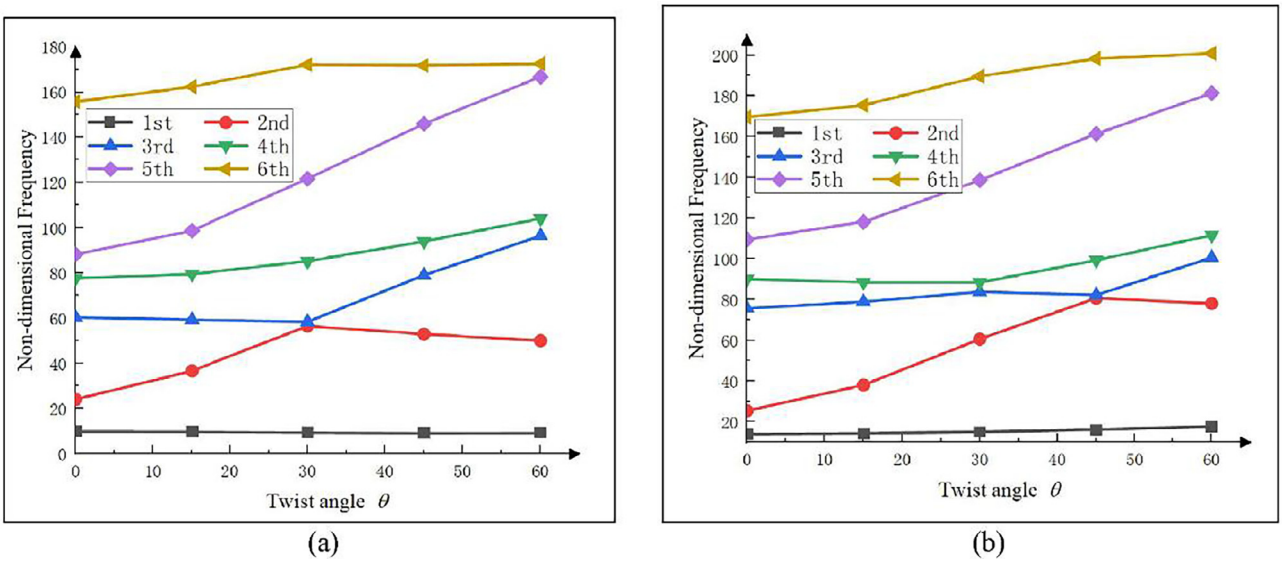

Fig. 12. First six non-dimensional frequencies versus twist angle for the pre-twisted blade, (a) $\gamma = 0$; (b) $\gamma = 8$.

$$\mathbf{V}_r = \boldsymbol{\Omega} \times (\mathbf{r} + R\mathbf{i}_x) = \frac{\Omega}{A}\begin{bmatrix} A(\eta+v)\sin\psi + (u\eta q + \zeta + w)\cos\psi \\ [-A(x+R) - u + \eta q(\zeta + w)]\sin\varphi \\ [-A(x+R) - u + \eta q(\zeta + w)]\cos\varphi \end{bmatrix}^T \begin{pmatrix} \mathbf{i}_x \\ \mathbf{i}_y \\ \mathbf{i}_z \end{pmatrix} \tag{33}$$

The kinetic energy of the blade is obtained as follows

$$T = \frac{1}{2}\iint_s \int_{-h/2}^{h/2} \rho A[(\dot{u} + \mathbf{V}_r\cdot\mathbf{e}_{0x})^2 + (\dot{v} + \mathbf{V}_r\cdot\mathbf{e}_{0\eta})^2 + (\dot{w} + \mathbf{V}_r\cdot\mathbf{e}_{0\zeta})^2]\, dx\, d\eta\, d\zeta$$
$$= \frac{1}{2}\iint_s \int_{-h/2}^{h/2} \rho A\left[\left(\dot{u} + \frac{V_x}{A} - \frac{\eta q V_g\cos\psi}{A}\right)^2 + (\dot{v} + V_g\sin\psi)^2 + \left(\dot{w} - \frac{V_x\eta q}{A} - \frac{V_g\cos\psi}{A}\right)^2\right] dx\, d\eta\, d\zeta \tag{34}$$

in which

$$V_g = \frac{\Omega}{A}[-A(x+R) - u + \eta q(\zeta + w)] \tag{35}$$

$$V_x = \Omega(\eta + v)\sin\psi + \frac{\Omega}{A}(u\eta q + \zeta + w)\cos\psi \tag{36}$$

The virtual work done by the external transverse force is written as

$$\delta W = \int_V F_w \delta w\, dV \tag{37}$$

where F_w is the external harmonic force normal to the blade surface.

Applying the Hamilton's principle, the variational form of the total energy can be derived as

$$\delta\int_{t_1}^{t_2} (T - U_S - U_{CF} + W)dt = 0 \tag{38}$$

2.5. Frequency solving

In this paper, numerical simulations are employed to study the free vibration of a pre-twisted blade. In order to ensure the safety and serviceability during the service life of the blade, it is required to know the natural frequencies of the blade to avoid resonance with external

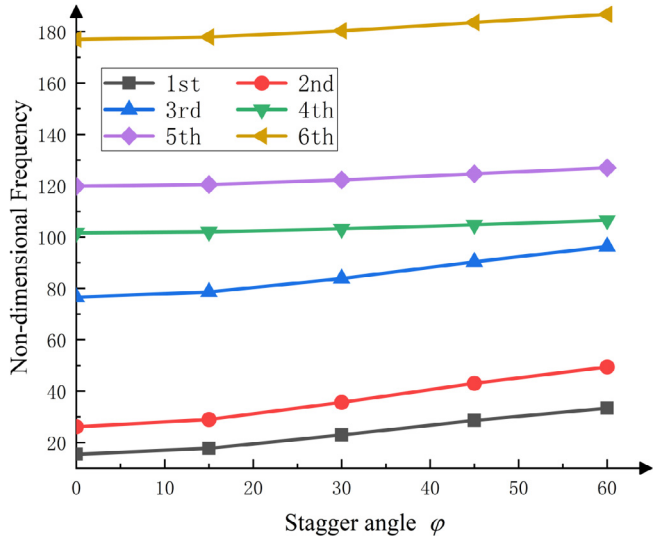

Fig. 13. First six non-dimensional frequencies versus stagger angle for the blade with $\gamma = 10$.

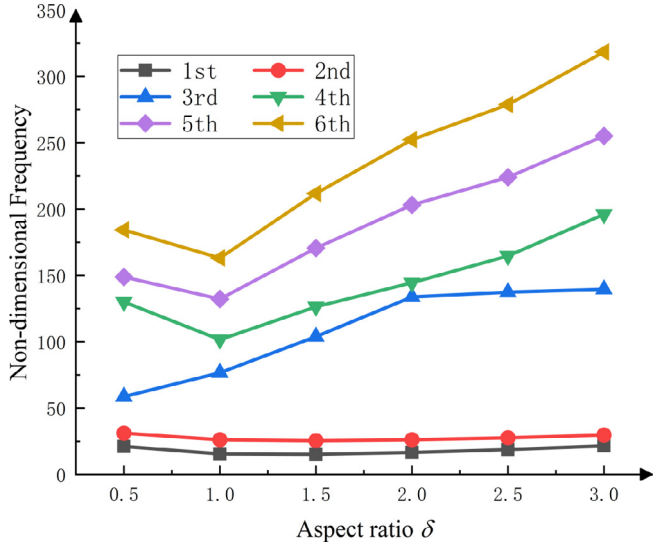

Fig. 14. First six non-dimensional frequencies versus aspect ratio for the blade with $\gamma = 10$.

excitation frequencies. The Rayleigh-Ritz method is employed to determine the natural frequencies and mode shapes of the pre-twisted composite laminated blade. The expressions of the displacements are assumed by the following forms

$$u(x, \eta, t) = U(x, \eta)e^{i\omega t} \tag{39}$$

$$v(x, \eta, t) = V(x, \eta)e^{i\omega t} \tag{40}$$

$$w(x, \eta, t) = W(x, \eta)e^{i\omega t} \tag{41}$$

where ω is the natural frequency of the pre-twisted blade. The algebraic polynomial functions $U(x, \eta)$, $V(x, \eta)$ and $W(x, \eta)$ represent the mode shapes and can guarantee convergence to the exact solution as the number of terms increases [39]. Besides the mode shapes should be satisfied the geometric boundary conditions of a cantilever, i.e., one edge is clamped and the other three edges are free. Hence, the mode shapes are expended as

$$U(\xi, \chi) = \sum_{i=1}^{I} \sum_{j=0}^{J} A_{ij}\xi^i\chi^j \tag{42}$$

$$V(\xi, \chi) = \sum_{k=1}^{K} \sum_{l=0}^{L} B_{kl}\xi^k\chi^l \tag{43}$$

$$W(\xi, \chi) = \sum_{m=2}^{M} \sum_{n=0}^{N} C_{mn}\xi^m\chi^n \tag{44}$$

where $\xi = \frac{x}{L}$ and $\chi = \frac{2\eta}{b}$ are the dimensionless coefficients. A_{ij}, B_{kl} and C_{mn} are undetermined coefficients. (I, J), (K, L) and (M, N) are the number of the polynomial expansion, which must be selected with care to achieve the required accuracy. It should be stated that the Rayleigh-Ritz method requires satisfaction of geometric boundary conditions. The indices in Eqs. (42)–(44) begin with $i = 1$, $k = 1$ and $m = 2$ can ensure satisfaction of the clamped boundary conditions $\left(u = v = w = \frac{\partial w}{\partial x} = 0\right)$ at $\xi = 0$ for all terms of the polynomials [38,39].

Substituting Eqs. (21)–(23) into Eq. (24) and respectively, one can obtain the maximum kinetic energy and the maximum potential energy by setting $t = 0$. Then the Rayleigh-Ritz method is applied to achieve the following derivations.

$$\frac{\partial(T_{\max} - U_{\max})}{\partial A_{ij}} = 0, \quad (i = 1, ...I; j = 1, ...J) \tag{45}$$

$$\frac{\partial(T_{\max} - U_{\max})}{\partial B_{kl}} = 0, \quad (k = 1, ...K; l = 1, ...L) \tag{46}$$

$$\frac{\partial(T_{\max} - U_{\max})}{\partial C_{mn}} = 0, \quad (m = 1, ...M; n = 1, ...N) \tag{47}$$

The solution of the above equations can be described by

$$(\mathbf{K} - \omega^2\mathbf{M})[\mathbf{X}] = \mathbf{F} \tag{48}$$

where vector $[\mathbf{X}] = [U_{ij} \quad V_{kl} \quad W_{mn}]^T$, $\mathbf{K}$ and $\mathbf{M}$ are the stiffness and mass matrices, respectively. In the case of free vibration, the external force is assumed to be zero, $\mathbf{F} = 0$. But the Coriolis effects are still included, leading to a complex eigenvalue problem. The generalized eigenvalues (natural frequencies) can be obtained by setting the coefficient matrix of Equation to be zero, and the corresponding mode shapes can be obtained by substituting the eigenvector $[\mathbf{X}]$ back into Eqs. (42)–(44).

All the numerical results are presented in dimensionless forms as

$$\delta = \frac{L}{b}, \quad \sigma = \frac{R}{L}, \quad \lambda = \frac{h}{L}, \quad \gamma = \Omega\left(\frac{\rho L^4 h}{D_{11}}\right)^{1/2}, \quad \mu = \omega\left(\frac{\rho L^4 h}{D_{11}}\right)^{1/2} \tag{49}$$

where $D_{11} = E_1 h^3/12(1-\upsilon_{12}\upsilon_{21})$. δ, λ and ϑ donate the aspect ratio, thickness ratio and hub radius ratio of the composite laminated blade, respectively. μ and γ represent the dimensionless natural frequency and rotation speed.

3. Numerical results

3.1. Convergence and comparison study

The validity of the present modeling method is verified by comparing the first six non-dimensional frequencies obtained by the developed model with those in literature [30]. The same material properties as those in reference [30] are adopted. The corresponding comparison results are shown in Table 1. It can be found that the lowest six non-dimensional frequencies obtained in this study are in good agreement with those in literature.

The results of convergence study are given in Table 2. The number of terms chosen for components of the displacements in ξ-direction and χ-direction is the same [39]. It is found that when the number of terms considered in the numerical calculation is more than 6×6 for each component of the displacements U, V and W, a consistent convergence can be observed. Increasing the number of the mode functions will multiply the computational time with little improvement in accuracy.

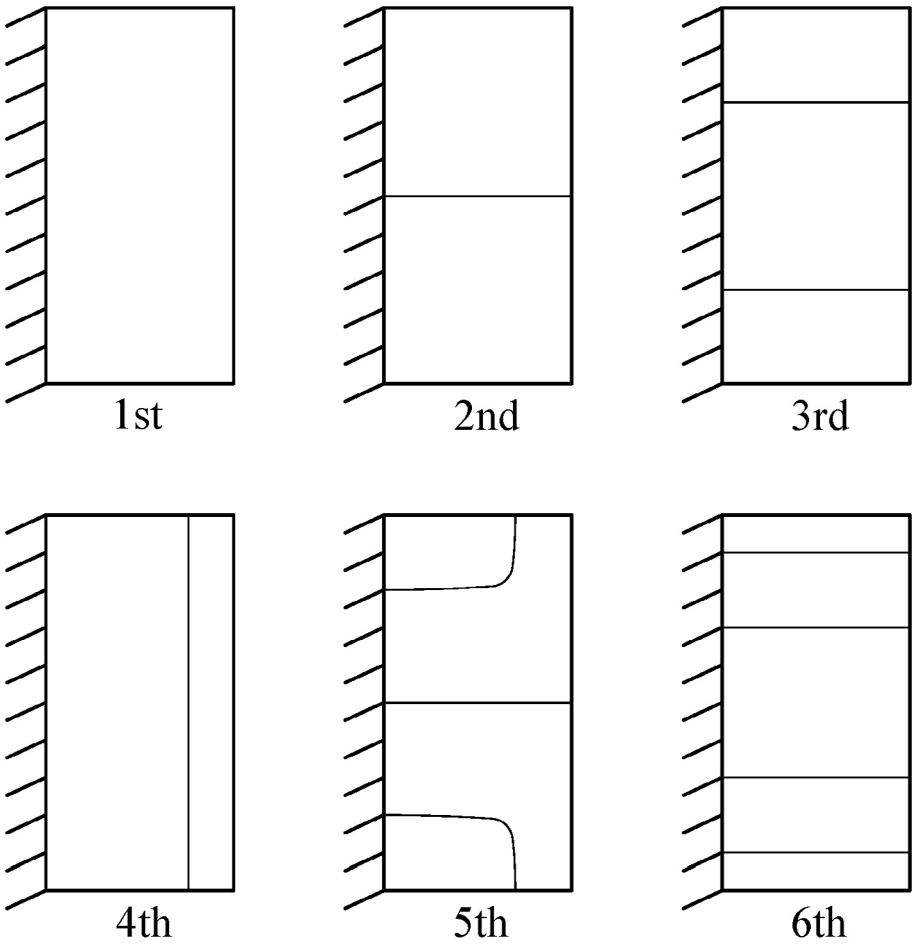

Fig. 15. Nodal lines of the first six mode shapes for the blade with aspect ratio $\delta = 0.5$.

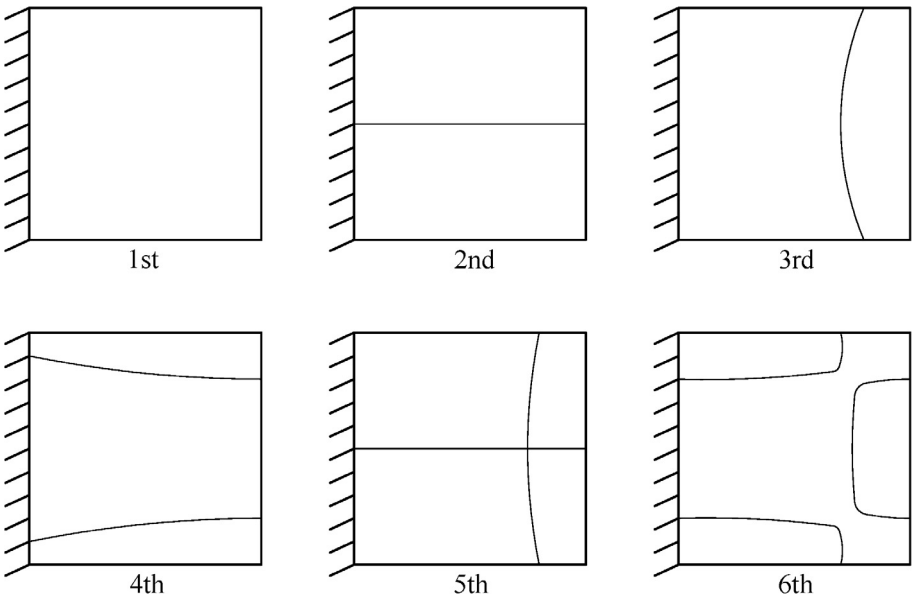

Fig. 16. Nodal lines of the first six mode shapes for the blade with aspect ratio $\delta = 1$.

Hence, $3 \times 6 \times 6$ mode functions are employed in the following analysis.

The first six non-dimensional frequencies and corresponding mode shapes are compared with the numerical results of the finite element method based on ANSYS. The dimensional parameters and material properties of the symmetric cross-ply composite laminated blade are selected as $\delta = 1$, $\vartheta = 0$, $\lambda = 0.01$, $\theta = 0°$, $\varphi = 0°$, $\rho = 1700kg/m^3$, $E_1 = 1.4 \times 10^{11}N/m^2$, $E_2 = 9.1 \times 10^9N/m^2$, $G_{12} = 7.2 \times 10^9N/m^2$, $\upsilon_{12} = 0.2$ and $\upsilon_{21} = 0.3$. The cross-ply composites are made of six layers (0/90/0/0/90/0)s and all layers have the same thickness [38]. The comparison of the first six non-dimensional frequencies are shown in Table 3. Figs. 2 and 3 show the first six mode shapes of the pre-twisted composite laminated blade. It can be observed that the first and third modes are the first two bending modes, the second and fourth modes

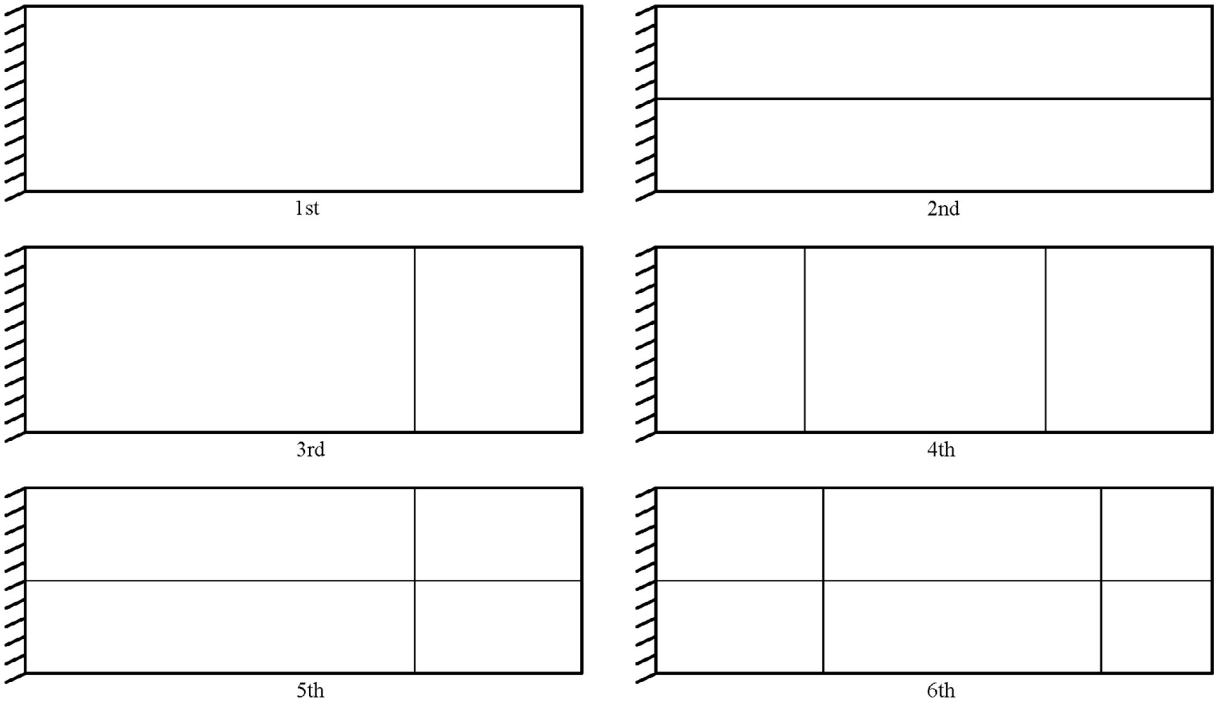

Fig. 17. Nodal lines of the first six mode shapes for the blade with aspect ratio $\delta = 3$.

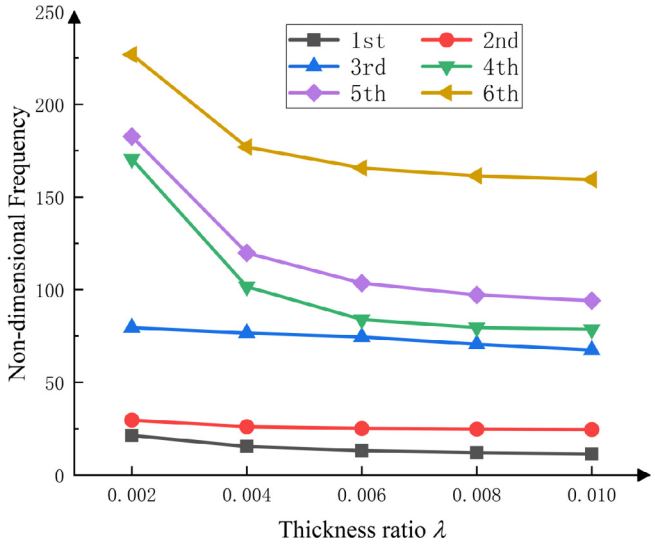

Fig. 18. First six non-dimensional frequencies versus thickness ratio for the blade with $\gamma = 6$.

are the first two torsional modes. The other two modes are coupled bending and torsional modes. A good agreement of the first six mode shapes can also be found. The aforementioned comparison and convergence studies demonstrate the validity of the present modeling method.

3.2. Free vibration of the composite laminated blade

In this section, the effects of different parameters on the free vibrations of the composite laminated pre-twisted blade are studied. The parameters and other information of the blade are the same as those in the last comparison case in Section 3.1. Fig. 4 shows the corresponding first six non-dimensional frequencies of the rotating blade versus the non-dimensional rotation velocity. It is observed from Fig. 4 that all the non-dimensional frequencies increase as the rotation velocity increases. This is attributed to the effect of centrifugal force, which increases the bending stiffness as the rotation velocity increases.

It is worth noting that the frequency loci veering phenomenon which was discussed by Leissa [40] for rotating structures can be observed from Fig. 4. The third and fourth frequencies approach each other and then veer away with increasing of the rotation velocity. Fig. 5 indicates the corresponding third and fourth mode shapes of the composite laminated blade with different rotation velocities. Fig. 5(a) and (b) respectively show the third mode shape for the non-dimensional rotation velocity $\gamma = 4$ and $\gamma = 8$, respectively. Fig. 5(c) and (d) represent the fourth mode shape for the non-dimensional rotation velocity $\gamma = 4$ and $\gamma = 8$, respectively. It can be observed from Fig. 5 that the third mode of the blade is dominated by bending vibration and the fourth mode is dominated by torsional vibration. However, when $\gamma = 8$ the third mode changes from the bending dominated mode into the torsional dominated mode, while the fourth mode becomes the bending dominated mode. This is attributed to that the centrifugal forces have a greater influence on the bending dominated mode than the torsional dominated mode. Therefore, the frequencies corresponding to the bending dominated mode increase faster than those corresponding to the torsional dominated mode [23]. The switching shapes of the third and fourth modes shown in Fig. 5 verify the associated frequency loci veering phenomenon shown in Fig. 4.

The frequency loci veering phenomenon can be further explained according to the nodal line patterns of the frequencies loci. Figs. 6 and 7 demonstrate the corresponding first six nodal line patterns of the composite laminated blade for $\gamma = 4$ and $\gamma = 8$, respectively. It can be observed that the nodal line patterns of the third and fourth modes exchange each other. Herein the critical non-dimensional rotation velocity is $\gamma = 6.2$ as shown in Fig. 8. The variation of the nodal lines with the non-dimensional rotation velocity for the third and fourth modes are displayed in Fig. 8. It is obvious that the mode switching occurs continuously and all the modal lines of the two mode shapes pass through two fix points with an increase of rotation velocity. A similar phenomenon was reported by Yoo et al. [1].

The effect of pre-twisted angle on the frequency of the pre-twisted composite laminated blade is considered herein. Fig. 9 indicates the first six non-dimensional frequencies of the rotating blade versus the

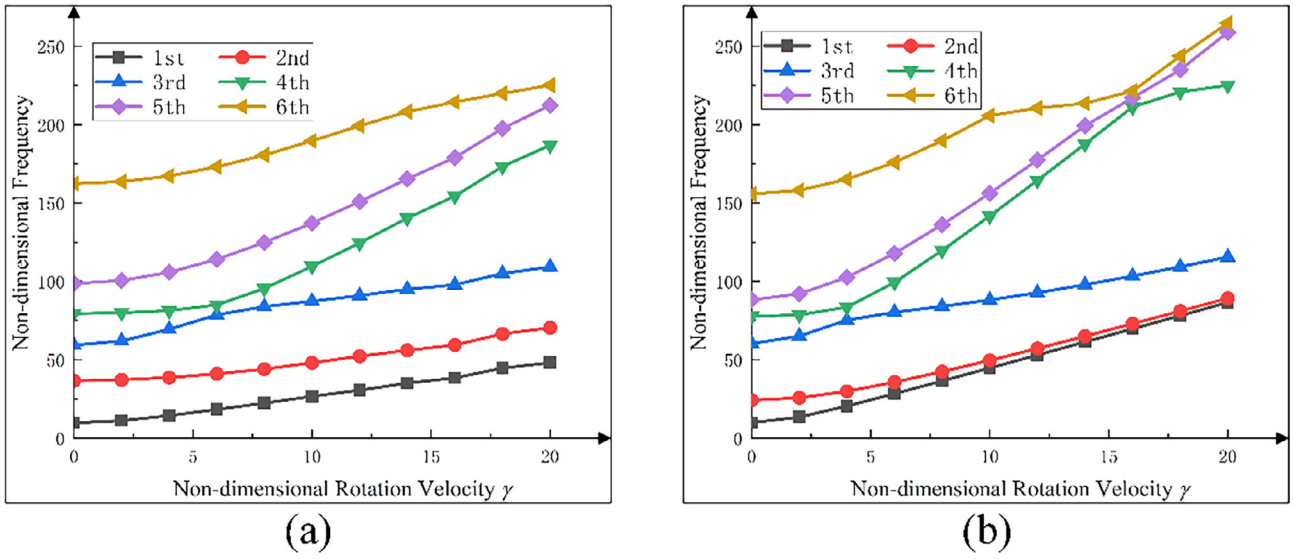

Fig. 19. First six non-dimensional frequencies versus rotation velocity for the blade, (a) hub radius ratio $\vartheta = 0.2$; (b) hub radius ratio $\vartheta = 1$.

non-dimensional rotation velocity for pre-twisted angle $\theta = 45°$. It is found that the frequency veering phenomenon comes up between the second, third and fourth modes. The third mode firstly exchanges with the second mode when $\gamma = 14$, then exchanges its mode with the fourth mode when $\gamma = 18$. Fig. 10 shows the corresponding mode shapes in detail. Fig. 10(a–c) show the second, third and fourth mode shapes when $\gamma = 12$. Fig. 10(d–f) and (g–i) show the corresponding mode shapes for $\gamma = 14$ and $\gamma = 19$, respectively. The variation of the modal lines for the third mode versus the non-dimensional rotation velocity is displayed in Fig. 11. It can be observed that the mode exchanges between the first torsional mode and the first bending mode occurs in abrupt. However, the changes of the first bending mode and second torsional mode are continuous. Fig. 12(a) and (b) show the first six non-dimensional frequencies versus the twisted angle for $\gamma = 0$ and $\gamma = 8$, respectively. It can be observed that the twist angle of the blade does not have any obvious effects on the first frequency. However, with an increase of twist angle, the other frequencies increase.

The effect of the stagger angle φ on the first six frequencies of the blade when $\gamma = 10$ is shown in Fig. 13. It indicates that the effect of the stagger angle on the frequencies is not as significant as the twist angle. The first six frequencies of the blade increase slightly as the stagger angle augments.

The effect of the aspect ratio δ on the variations of the frequencies is shown in Fig. 14. It can be found from the figure that the aspect ratio has little effect on the first two frequencies. However, the next four frequencies increase as the aspect ratio increases. Figs. 15–17 respectively show the six mode shapes for $\delta = 0.5$, $\delta = 1$ and $\delta = 3$. It can be observed that the first two mode shapes for these aspect ratios are the same, which corresponding to the little change of the first two frequencies versus the aspect ratio shown in Fig. 14. However, the third to the sixth mode shapes are totally different under these aspect ratios.

The effect of the thickness ratio λ on the variations of the first six frequencies when $\gamma = 6$ is shown in Fig. 18. As expected, the non-dimensional frequencies decrease as the thickness ratio increases. Besides, the decreasing rate of frequencies become larger as the order of the frequency increases. That means the effect of the thickness ratio on the higher order frequencies is more significant than that on the lower order ones.

Fig. 19 demonstrates the variations of the first six non-dimensional frequencies of the blade for hub radius ratio $\vartheta = 0.2$ and $\vartheta = 1$. The frequencies increase as the rotation velocity increases for these two cases. However, the rate of increase becomes higher as the hub radius ratio σ increases. That is because the centrifugal inertia force increases if the hub radius increases as well as the rotation velocity.

4. Conclusion

In this paper, a dynamic model based on the shell theory was developed to investigate the vibration characteristics of a rotating composite laminated blade. The natural frequencies of a rotating pre-twisted composite laminated blade were obtained by the Rayleigh-Ritz method. The convergence and comparison studies demonstrated the accuracy and validity of the present modeling method.

The effects of the rotation velocity on the natural frequencies and the corresponding mode shapes of the blade were discussed. Due to the effects of the Coriolis and centrifugal forces, variation of different natural frequencies with rotation velocity was diverse, resulting in the phenomena of frequency loci veering and crossing. Two ways of frequency loci veer can be observed. For the first one, the nodal line patterns of the mode shapes switch their shapes to each other continuously. For the other one, the nodal line patterns vary in abrupt and discontinuously.

A comprehensive parameter investigation of the effects of the aspect ratio, pre-twisted angle, stagger angle and hub radius on the variations of modal characteristics was conducted. Numerical results demonstrated that the natural frequencies of the rotating blade increase as the pre-twisted angle, stagger angle and the hub radius increase, while decrease as the thickness ratio increases.

It was demonstrated through the results of this paper that the proposed model is an efficient tool for predicting the dynamic behavior of blades with arbitrary geometry dimension, stagger angle and pre-twisted angle, which will provide useful information for the design and optimization of the blades. Based on the results of this paper, further investigations will extend to the internal resonances and nonlinear dynamics of the composite laminated blades rotating at high rotation velocity.

Acknowledgment

The work described in this paper was fully supported by a grant from the Fundamental Research Program of Shenzhen Municipality (Project No: JCYJ20160608153749600).

References

[1] Yoo HH, Pierre C. Modal characteristic of a rotating rectangular cantilever plate. J

Sound Vib 2003;259:81–96.
[2] Yao MH, Chen YP, Zhang W. Nonlinear vibrations of blade with varying rotating speed. Nonlinear Dyn 2012;68:487–504.
[3] Yao MH, Zhang W, Chen YP. Analysis on nonlinear oscillations and resonant responses of a compressor blade. Acta Mech 2014;225:3483–510.
[4] Lee SY, Lin SM, Wu CT. Free vibration of a rotating non-uniform beam with arbitrary pretwist, an elastically restrained root and a tip mass. J Sound Vib 2004;273:477–92.
[5] Lin SM. The instability and vibration of rotating beams with arbitrary pretwist and an elastically restrained root. J Appl Mech 2000;68:844–53.
[6] Liu TR, Ren YS. Vibration of wind turbine blade modeled as composite thin-walled closed-section structure. Advanced Materials Research 2010;129–131:23–7.
[7] Yoo HH, Kwak JY, Chung J. Vibration analysis of rotating pre-twisted blades with a concentrated mass. J Sound Vib 2001;240:891–908.
[8] Librescu L, Oh SY, Song O, Kang HS. Dynamics of advanced rotating blades made of functionally graded materials and operating in a high-temperature field. J Eng Math 2008;61:1–16.
[9] Oh SY, Librescu L, Song O. Vibration of turbomachinery rotating blades made-up of functionally graded materials and operating in a high temperature field. Acta Mech 2003;166:69–87.
[10] Librescu L, Oh SY, Song O. Thin-walled beams made of functionally graded materials and operating in a high temperature environment: vibration and stability. J Therm Stresses 2005;28:649–712.
[11] Lin CY, Chen LW. Dynamic stability of rotating pre-twisted blades with a constrained damping layer. Compos Struct 2003;61:235–45.
[12] Subrahmanyam KB, Kulkarni SV, Rao JS. Coupled bending-bending vibrations of pre-twisted cantilever blading allowing for shear deflection and rotary inertia by the Reissner method. Int J Mech Sci 1981;23:517–30.
[13] Banerjee JR. Development of an exact dynamic stiffness matrix for free vibration analysis of a twisted Timoshenko beam. J Sound Vib 2004;270:379–401.
[14] Hajianmaleki M, Qatu MS. Vibrations of straight and curved composite beams: A review. Compos Struct 2013;100:218–32.
[15] Hajianmaleki M, Qatu MS. Static and vibration analyses of thick, generally laminated deep curved beams with different boundary conditions. Compos B Eng 2012;43:1767–75.
[16] Sinha SK, Turner KE. Natural frequencies of a pre-twisted blade in a centrifugal force field. J Sound Vib 2011;330:2655–81.
[17] Yoo HH, Kim SK, Inman DJ. Modal analysis of rotating composite cantilever plates. J Sound Vib 2002;258:233–46.
[18] Yoo HH, Kim SK. Free vibration analysis of rotating cantilever plates. AIAA Journal 2002;40:2188–96.
[19] Fang JS, Zhou D. Free vibration analysis of rotating mindlin plates with variable thickness. Int J Struct Stab Dyn 2016;17:1750046.
[20] Mishra I, Sahu SK. Modal analysis of woven fiber composite plates with different boundary conditions. Int J Struct Stab Dyn 2014;15:1540001.
[21] Civalek Ö. Numerical solutions to the free vibration problem of Mindlin sector plates using the discrete singular convolution method. Int J Struct Stab Dyn 2009;09:267–84.
[22] Hashemi SH, Farhadi S, Carra S. Free vibration analysis of rotating thick plates. J Sound Vib 2009;323:366–84.
[23] Zhao J, Tian Q, Hu H. Modal analysis of a rotating thin plate via absolute nodal coordinate formulation. J Comput Nonlinear Dyn 2011;6:041013–8.
[24] Sun J, Kari L, Lopez Arteaga I. A dynamic rotating blade model at an arbitrary stagger angle based on classical plate theory and the Hamilton's principle. J Sound Vib 2013;332:1355–71.
[25] Li L, Zhang DG. Free vibration analysis of rotating functionally graded rectangular plates. Compos Struct 2016;136:493–504.
[26] Jang JH, Kim JH. Nonlinear modeling and coupled characteristic of composite structure with complex curvature. Int J Precis Eng Manuf 2012;13:2027–33.
[27] Sun J, Lopez Arteaga I, Kari L, General. shell model for a rotating pretwisted blade. J Sound Vib 2013;332:5804–20.
[28] Sun J, Lopez Arteaga I, Kari L. Dynamic modeling of a multilayer rotating blade via quadratic layerwise theory. Compos Struct 2013;99:276–87.
[29] Sinha SK, Zylka RP. Vibration analysis of composite airfoil blade using orthotropic thin shell bending theory. Int J Mech Sci 2017;121:90–105.
[30] Kee YJ, Kim JH. Vibration characteristics of initially twisted rotating shell type composite blades. Compos Struct 2004;64:151–9.
[31] Gulyaev VI, Khudolii SN. Vibrations of curved and twisted blades during complex rotation. Int Appl Mech 2005;41:449–54.
[32] Zhang XM. Parametric analysis of frequency of rotating laminated composite cylindrical shells with the wave propagation approach. Comput Methods Appl Mech Eng 2002;191:2057–71.
[33] Rao J, Gupta K. Free vibrations of rotating small aspect ratio pretwisted blades. Mech Mach Theory 1987;22:159–67.
[34] Lim CW. A spiral model for bending of non-linearly pretwisted helicoidal structures with lateral loading. Int J Solids Struct 2003;40:4257–79.
[35] Qatu MS. Vibration of Laminated Shells and Plates. Elsevier; 2004.
[36] Amabili M. Nonlinear Vibrations and Stability of Shells and Plates. Cambridge University Press; 2008.
[37] Gupta K, Rao J. Torsional vibrations of pretwisted cantilever plates. J Mech Des 1978;100:528–34.
[38] Reddy JN. Mechanics of Laminated Composite Plates and Shells: Theory and Analysis. CRC Press; 2004.
[39] Qatu MS, Leissa AW. Vibration studies for laminated composite twisted cantilever plates. Int J Mech Sci 1991;33:927–40.
[40] Leissa AW. On a curve veering aberration, Zeitschrift für angewandte Mathematik und Physik. ZAMP 1974;25:99–111.